LUMIO: Characterizing Lunar Meteoroid Impacts with a CubeSat

Topputo, Francesco; Cervone, Angelo; Sundaramoorthy, Prem; Speretta, Stefano; Mestry, Samiksha; Noomen, Ron; More Authors

IAC-18,A3,2A,7,x47249

LUMIO: CHARACTERIZING LUNAR METEOROID IMPACTS WITH A CUBESAT

**F. Topputo [(1)], M. Massari [(1)], J. Biggs [(1)], P. Di Lizia [(1)], D. A. Dei Tos [(1)(*)], K. V. Mani [(1)],
S. Ceccherini [(1)], V. Franzese [(1)], A. Cervone [(2)], P. Sundaramoorthy [(2)], S. Speretta [(2)],
S. Mestry [(2)], R. Noomen [(2)], A. Ivanov [(3)], D. Labate [(4)], A. Jochemsen [(5)], R. Furfaro [(6)],
V. Reddy [(6)], K. Jacquinot [(6)], R. Walker [(7)], J. Vennekens [(7)], A. Cipriano [(7)], D. Koschny [(7)]**

[(1)] *Politecnico di Milano, Via La Masa 34, 20156, Milano, Italy*
[(2)] *TU Delft, Kluyverweg 1, 2629, Delft, The Netherlands*
[(3)] *École Polytechnique Fédérale de Lausanne, Route Cantonale, 1015, Lausanne, Switzerland and Skolkovo Institute of Science and Technology, Moscow, Russian Federation*
[(4)] *Leonardo, Via delle Officine Galileo 1, 50013, Campi Bisenzio, Florence, Italy*
[(5)] *Science and Technology AS, Tordenskiolds Gate 3, 0160, Oslo, Norway*
[(6)] *University of Arizona, 1130 N Mountain Ave., 85721, Tucson, AZ, United States*
[(7)] *ESA/ESTEC, Keplerlaan 1, 2201 AZ, Noordwijk, The Netherlands*
[(*)] Corresponding Author

Abstract

The Lunar Meteoroid Impact Observer (LUMIO) is a mission designed to observe, quantify, and characterize the meteoroid impacts by detecting their flashes on the lunar farside. Earth-based lunar observations are restricted by weather, geometric, and illumination conditions, while a lunar orbiter can improve the detection rate of lunar meteoroid impact flashes, as it would allow for longer monitoring periods. This paper presents the scientific mission of LUMIO, designed for the ESA SysNova LUCE competition, that resulted as the ex-aequo winner in the competition. LUMIO, a 12U CubeSat weighting approximately 20 kg, is expected to be deployed into a quasi-polar selenocentric orbit by a mother spacecraft, which also acts as communication relay. From a lunar high-inclination orbit, LUMIO will autonomously determine its trajectory to reach the Moon–Earth L_2 point and perform the cruise phase. From the operative orbit, LUMIO will observe the lunar farside. When the lunar disk illumination is less than 50%, LUMIO autonomously performs the scientific task without direct coordination from Earth. Fully autonomous operations will include science, communication, and navigation. A similar concept can be re-used for a wide variety of future missions. The scientific mission will also be possible thanks to an innovative on-board data processing system, capable of drastically reducing the information to transmit to Earth. The camera, designed to capture the flashes and measure their intensity is, in fact, capable of generating 2.6 TB/day while only approximately 1 MB/day will need to be transmitted to Earth. Impact identification will be autonomous and only relevant information will be transmitted. A study at the ESA/ESTEC concurrent design facility has shown evidence of feasibility and that a CubeSat orbiting along an Earth–Moon L_2 quasi-halo orbit is expected to bring a relevant contribution to lunar science and innovation to space exploration.

Keywords: LUMIO, CubeSat, Meteoroid impact flash, Lunar Situational Awareness, Earth–Moon L_2, ESA SysNova challenge

1. Introduction

1.1 Scientific relevance

Impacts due to near Earth objects (NEO) could cause a devastating humanitarian crisis and potentially the extinction of humanity. While the probability of such an event is very low, the outcome is so catastrophic that it is imperative to invest resources to mitigate them. Telescopic surveys detect NEO greater than 1 km down to 1 meter in size, but there are few direct methods for monitoring the sub-meter meteoroid population. Serendipitous monitoring of atmospheric explosions due to airbursts of meteoroids are being undertaken. These objects are part of the ~33 metric tons of debris impacting the Earth each day.

Meteoroids are small Sun-orbiting fragments of asteroids and comets, whose sizes range from micrometers to meters and masses from 10^{-15} to 10^4 kg [1]. Formation of meteoroids is a consequence of asteroids colliding with each other and/or with other bodies, comets releasing dust particles when close to the Sun, and minor bodies shattering into individual fragments. Meteoroids are hardly detectable even with dedicated surveys. However, they may be observed indirectly when an impact occurs with a planetary or moon solid surface. An impact represents in fact a unique opportunity to understand and update the models

describing the spatial distribution of NEO in the solar system, which is critical for several reasons. The ability to accurately and timely predict these impacts by relying on accurate meteoroid impact flux models is fundamental in many fields.

1.2 Lunar meteoroid impacts

Current estimations of the larger-than-1-kg meteoroid flux at the Moon varies across the literature. 1290 impacts per year are estimated [2], while estimates approximately 4000 impacts per year [3] [4]. More recent studies suggest that the meteoroid impact flux at the Moon is approximately 6×10^{-10} m^2/year, for meteoroids larger than 30 grams [5]. Assuming a lunar collecting area equal to its surface area, i.e., 3.8×10^{13} m^2, this gives a larger-than-30-grams meteoroid flux of approximately 23000 impacts per year.

There are also speculations on the possible asymmetries of the spatial distribution of impacts across the lunar surface. In [6], it is theorized that the Moon nearside has approximately 0.1% more impacts than the lunar farside, due to the Earth gravity field; the equatorial flux is 10–20% larger than that at polar regions, due to the higher number of large meteoroids in low orbital inclinations; and the lunar leading side (apex) encounters between 37 and 80% more impactors than the trailing side (antapex), due the Moon synchronous rotation.

In a lunar meteoroid impact, the kinetic energy of the impactor is partitioned into 1) the generation of a seismic wave, 2) the excavation of a crater, 3) the ejection of particles, and 4) the emission of radiation. Any of these phenomena can be observed to detect lunar meteoroid impacts. The detection of lunar impact flashes is the most advantageous method since it yields an independent detection of meteoroid impacts, provides the most complete information about the impactor, and allows for the monitoring of a large Moon surface area [7]. Remote observation of light flashes is thus baselined for the detection of lunar meteoroid impacts.

1.3 Sun–Earth–Moon geometry

The Moon spin–orbit motion is locked into a 1:1 resonance, meaning that an observer on Earth always sees the same portion of the Moon, that is the lunar nearside. This characteristic, in addition to the fact that a fixed observer on Earth also moves with respect to the Moon, as the Earth rotates about its own axis, constrains the observation of the Moon from Earth.

Since the Moon–Sun synodic period is 29.53 days, the illumination of the lunar nearside varies and originates the Moon phases. Because lunar impact flashes can only be observed from ground on the lunar night side and when the lunar nearside is less than 50% illuminated, flash detection from Earth is constrained by the Sun–Earth–Moon geometry. An observer of the lunar farside would also be constrained by the Sun–Moon geometry,

but would see temporally opposite phases. As such, assuming that the lunar farside would also have to be less than 50% illuminated, the observations would occur during the opposite time of the month. Fig. 1 shows the Moon phases and main directions of incoming meteoroids in the Earth–Moon system (North and South Toroidal sources are perpendicular to the plane). The dashed green line represents the portion of the Moon orbit where Earth-based observations of the nearside can be made. The solid blue line indicates the portion of the Moon orbit where space-based observations of the farside can be made.
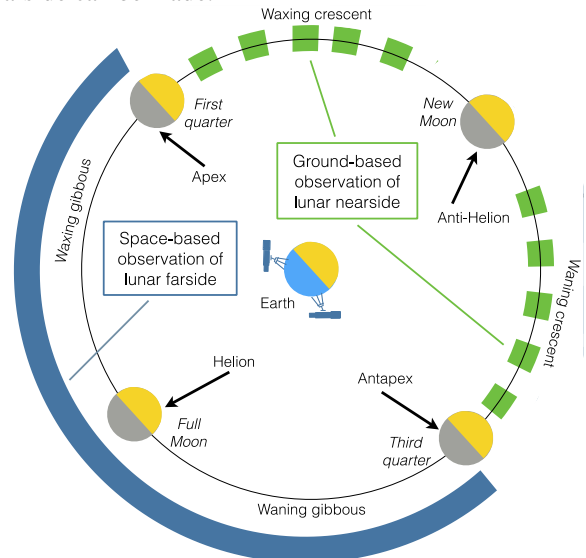

Fig. 1: Geometry for meteoroid impact flash detection.

Observing the lunar impacts with space-based assets yields several benefits over ground-based telescopes, namely:

- *No atmosphere*. Ground-based observations are biased by the atmosphere that reduces the light flash intensity depending upon present conditions, which change in time. This requires frequent recalibration of the telescope. Inherent benefits of the absence of atmosphere in space-based observations are twofold: 1) there is no need of recalibrating the instrument, and 2) fainter flashes may be detected.

- *No weather*. Ground-based observations require good weather conditions, the lack of which may significantly reduce the observation time within the available window. There is no such constraint in space-based observations.

- *No day/night*. Ground-based observations may only be performed during Earth night, significantly reducing the observation period within the available window. There is no such limitation when space-based observations are performed.

- *Full disk*. Ground-based observations are performed in the first and third quarter, when nearside illumination is 10–50%. Full-disk

observations during New Moon are not possible because of low elevation of the Moon and daylight. Space-based observations of the lunar farside can capture the whole lunar full-disk at once, thus considerably increasing the monitored area.

- *All longitudes*. Ground-based observations happening during the first and third quarter prevent from resolving the meteoroid flux across the central meridian. There is no such restriction in space-based full-disk observations.

Moreover, observing the lunar farside with space-based assets yields further benefits, that is:

- *No Earthshine*. By definition, there is no Earthshine when observing the lunar farside. This may yield a lower background noise, thus enabling the detection of fainter signals, not resolvable from ground.
- *Complementarity*. Space-based observations of the lunar farside complement ground-based ones
  - o in space. The two opposite faces of the Moon are monitored when the Moon is in different locations along its orbit;
  - o in time. Space-based observations are performed in periods when ground-based ones are not possible, and vice-versa.

High-quality scientific products can be achieved with space-based observations of the lunar farside. These may complement those achievable with ground-based ones to perform a comprehensive survey of the meteoroid flux in the Earth–Moon system.

1.4 Lunar meteoroid impact flash detection

Light flashes at the Moon are typically observed by detecting a local spike of the luminous energy in the visible spectrum when pointing a telescope at the lunar night side. The background noise is mainly composed by the Earthshine (Earth reflected light on the Moon surface) in the visible spectrum, and by thermal emissions of the Moon surface in the infrared spectrum [8]. Measurements with high signal-to-noise ratios (SNR) may be obtained through observations of the lunar night side [9]. The detected luminous energy spike is quantified using the apparent magnitude of the light flash.

Lunar impact flashes detected from Earth-based observations have apparent magnitude between +5 and +10.5 [6], corresponding to faint signals. Also, Earth-based observations of lunar impact flashes are restricted to periods when the lunar nearside illumination is 10–50% [3], [10]. The upper limit restriction is due to the day side of the Moon glaring the telescope field of view (FOV). The lower limit restriction of 10% corresponds to the New Moon phase. During this phase, the observations should be made when the Moon presents itself at low elevations in the sky (morning or evening), but the observation periods are too short to be useful [6], [10].

The first unambiguous lunar meteoroid impact flashes were detected during 1999's Leonid meteoroid showers and were reported in [9]. The first redundant detection of sporadic impacts was only reported six years later [3]. These events gave origin to several monitoring programs. In 2006, a lunar meteoroid impact flashes observation program was initiated at NASA Marshall Space Flight Center [10]. This facility can monitor 4.5×10^6 km^2 of the lunar surface, approximately 10 nights per month, subject to weather conditions. Approximately half of the impact flashes observations occur between the Last Quarter and New Moon (0.5 to 0.1 illumination fraction) and the other half between New Moon and First Quarter (0.1 to 0.5 illumination fraction). The former monitoring period occurs in the morning (waning phase) and the latter occurs in the evening (waxing phase), covering the nearside part of the eastern and western lunar hemisphere, respectively. 126 high-quality flashes were reported in [5], for 266.88 hours of monitoring, over a 5 years period. The magnitude range detected is between +10.42 and +5.07, which is estimated to correspond to an impactor kinetic energy range between 1.67×10^{-7} and 2.31×10^{-4} kton TNT. The most recent monitoring program, NELIOTA, was initiated on February 2017 in Greece under ESA funding. As of November 2017, 16 validated impacts have been detected over 35 hours of observations. The program aims to detect flashes as faint as +12 apparent visual magnitude [11] and is the first allowing the determination of the impact flash blackbody temperature, by observing both in the visible and infrared spectrum. Monitoring the Moon for impact flashes inherently imposes several restrictions that can be avoided if the same investigation is conducted with space-bases assets.

1.5 LUMIO mission

LUMIO is a CubeSat mission to a quasi-halo orbit at Earth–Moon L_2 that shall observe, quantify, and characterize meteoroid impacts on the lunar farside by detecting their impact flashes, complementing Earth-based observations on the lunar nearside, to provide global information on the lunar meteoroid environment and contribute to Lunar Situational Awareness (LSA). The LUMIO mission is conceived to address the following,

- *Science Question*: What are the spatial and temporal characteristics of meteoroids impacting the lunar surface?
- *Science Goal*. Advance the understanding of how meteoroids evolve in the cislunar space by observing the flashes produced by their impacts with the lunar surface.
- *Science Objective*. Characterize the flux of meteoroids impacting the lunar surface.

2. Payload

The observation of the light flashes produced by meteoroid impacts on the Moon far-side is performed

through the LUMIO-Cam, the main payload of LUMIO. The impact flashes on the Moon can be modelled as black body emissions [6], with temperatures between 2700 and 6000 K [8], and durations greater than 30 ms [5]. The lowest impact energies correspond to apparent magnitudes higher than +6 as seen from Earth. These characteristics drive the payload requirements, both in terms of the camera detection and optics, and payload physical properties such as total mass, volume, power consumption, and storage.

2.1 Detector

The baseline detector is the CCD201 of E2V L3Vision™ . This device is a 1024x1024 pixel frame-transfer sensor that uses a novel output arrangement, capable of operating at an equivalent output noise of less than one electron at pixel rates of roughly 15 MHz. This makes the sensor well-suited for scientific imaging where the illumination is limited and the frame rate is high, as it is for LUMIO. The sensitivity of this detector extends towards the near-infrared (NIR) region, which allows to better exploit the emission of radiation due to the impacts. The detector features are reported in Tab. 1.

Tab. 1: Properties of LUMIO-Cam detector.

Parameter	Value
Image area	13.3x13.3 mm
Active pixels	1024x1024
Pixel size	13.3x13.3 μm
Storage area	13.3x13.3 mm
Low noise gain	1–1000
Readout frequency	~15 MHz
Charge handling cap.	80 ke$^-$/pixel
Readout noise	< 1 e$^-$ rms

2.2 Optics

In view of LUMIO's operative orbit, for which the spacecraft-Moon range spans between 35525 and 86551 km, a minimum payload field of view of 5.6 deg is necessary to have always the Moon full disk view. To compensate for pointing errors, a 6-deg FOV is considered with a 127-mm focal length. The LUMIO-Cam optics features are shown in Tab. 2.

Tab. 2: Optics features.

FOV	Focal length	Aperture
6.0 deg	127 mm	55 mm

2.3 Mechanical layout

The mechanical layout of LUMIO-Cam is shown in Fig. 2. The mechanical layout includes a mechanical barrel supporting five lenses, an entrance baffle for out-of-field straylight reduction, a focal plane assembly, a proximity electronics box, and an external box for mechanical protection.
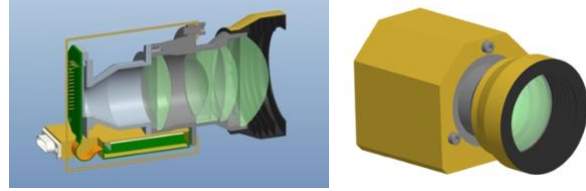

Fig. 2: LUMIO-Cam opto-mechanical assembly (left) and external box (right).

2.4 Budget

The mass and power budgets are reported in Tab. 3 and Tab. 4, respectively, where a 20% margin is considered owing to the early stage of the design. The LUMIO-Cam total margined mass is 1.56 kg and its worst-case power consumption (margined) is 4.2 W. In the power budget, the detector, the thermoelectric cooler (TEC), and the electronics are considered.

Tab. 3: Mass budget.

	Mass [kg]	Margin [%]	Margined mass [kg]
Lenses	0.3	20	0.36
Barrel	0.4	20	0.48
Baffle	0.1	20	0.12
Electronics	0.2	20	0.24
Box	0.3	20	0.36
Total	1.3	20	**1.56**

Tab. 4: Power budget.

	Power (Peak) [W]	Margin [%]	Margined power [W]
Detector	0.2	20	0.24
TEC	2.3 (2.8)	20	2.76 (3.36)
Electronics	0.5	20	0.6
Total	3.0 (3.5)	20	**3.6 (4.2)**

2.5 Radiometric analysis

A radiometric analysis employing the LUMIO-Cam properties is performed to assess the capability of the payload to detect the phenomenon under study. The detector collects photons emitted by the impact flash, but also some undesired signals, which are considered as noise, e.g., the straylight background noise, the dark current, the CCD readout noise. The SNR, output of the radiometric analysis, is higher than 5 dB, assuring the detectability of the range of meteoroid impact energies.

2.6 On-board payload data processing

On-board image processing is required due to the high amount of data generated by the payload. For an

acquisition rate of 1.8 MB images at 15 fps, the data products of the payload would be around 2.4 TB/day of science acquisitions. To reduce this amount, the on-board payload data processing (OBPDP) detects flashes in the images and stores only the images with scientific relevance. This leads to a reduction by a factor of about 23000. Since not all pixels of the full frame image are scientifically relevant data, the OBPDP also cuts everything outside an area around the flash. In this way, from 35.7 TB gathered during a LUMIO orbit period (~14.7 days), 13 MB of data needs to be stored (Fig. 3).

Fig. 3: Data amount reduction.

3. Mission analysis

It has been shown that remotely detecting flashes is the only technically and economically viable option for a CubeSat to monitor meteoroid impacts on the lunar surface [7]. When considering the conclusions of the preliminary and coverage trade-offs, the mission type flight heritage, and solar eclipse occurrences, the Earth–Moon L_2 halo family is baselined for the LUMIO mission. The vertical Lyapunov orbit family is selected as back-up plan but is not detailed in this paper. The mission is divided in four well defined phases (Fig. 4),

Parking:
  a. Starts when the lunar orbiter deploys LUMIO on the prescribed selenocentric elliptic parking orbit;
  b. Ends when LUMIO performs the stable manifold injection maneuver (SMIM);
  c. Lasts 14 days.

Transfer:
  a. Starts when LUMIO completes the SMIM;
  b. Ends when LUMIO performs the halo injection maneuver (HIM);
  c. Lasts 14 days.

Operative:
  a. Starts when LUMIO completes the HIM;
  b. The primary mission modes during the operative phase are Science Mode and Navigation and Engineering Mode (or Nav&Eng), alternating every halo period;
  c. Ends after one year of operations.

End of Life (EoL):
  a. De-commission of all (sub)systems;
  b. Ends when the EoL maneuver is correctly performed for safe disposal of the spacecraft.
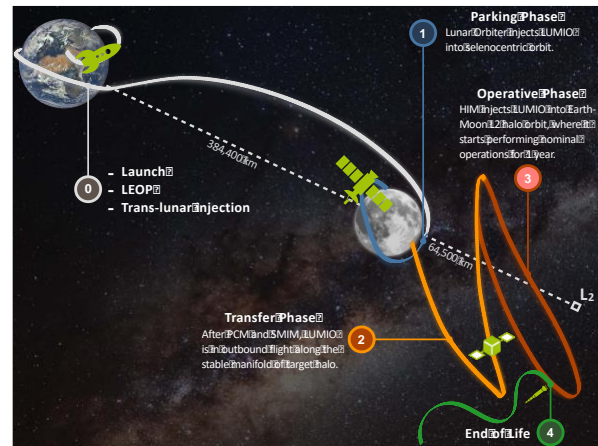

Fig. 4: Sketch of LUMIO mission phases.

3.1 Earth–Moon L_2 quasi-halos in high-fidelity model

A set of quasi-periodic halo orbits (sometimes referred here as quasi-halos or quasi-halo orbits) about the Earth–Moon L_2 are found by employing the methodology described in [12]. Fourteen quasi-halo orbits are computed in the high-fidelity roto-pulsating restricted *n*-body problem (RPRnBP) and saved as SPICE* kernels. The initial feeds to compute the quasi-halo samples are Earth–Moon three-body halos at 14 different Jacobi constants, ranging from $C_j = 3.04$ to $C_j = 3.1613263$. The latter value corresponds to the one assumed for the very first iteration of the activities. All orbits are computed starting from 2020 August 30 00:00:00.00 dynamical barycentric time (TDB). Although quasi-halos, shown in Fig. 5, are computed for a fixed initial epoch, the persistence of libration point orbits in the solar system ephemeris model allows wide freedom in the refinement algorithm, which also includes the mission starting at different epochs [13].

Quasi-halo orbits of Fig. 5 are all possible LUMIO operative orbits. As the orbit becomes more energetic (or as its CRTBP Jacobi constant decreases), the quasi-halo exhibits a wider range of motion both in terms of Moon range and of geometrical flight envelope about the corresponding circular restricted three-body problem (CRTBP) trajectory. The latter trend is disadvantageous when a hard-pointing constraint must be respected, e.g., Moon full disk on optical instrument. On the other hand, the lunar distance places a constraint on the minimum FOV for the optical instrument on board LUMIO to be able to resolve the Moon full disk at any location along the quasi-halo.

3.2 Orbital transfer to quasi-halo orbit

The transfer phase of LUMIO is done entirely in the CRTBP. Free transport mechanisms are leveraged to
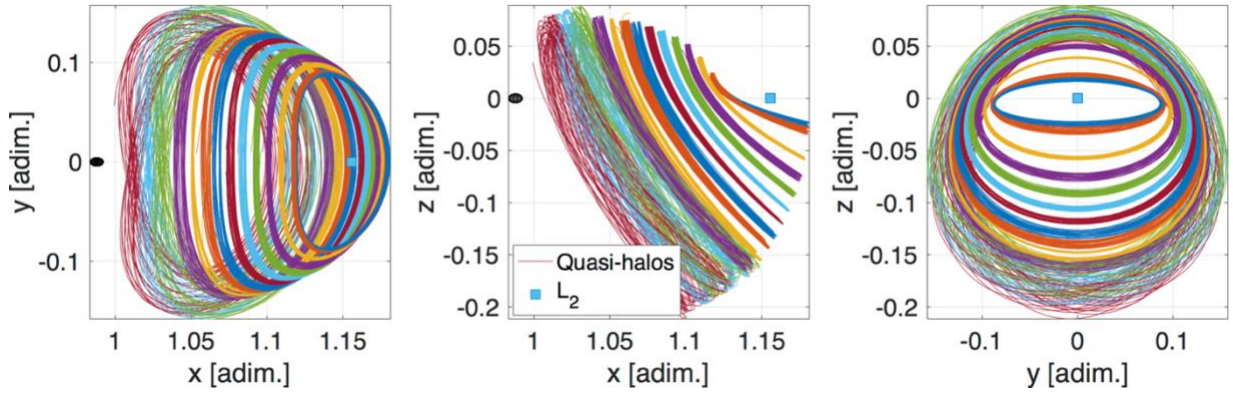
Fig. 5: Projection of Earth–Moon L_2 quasi-halos in the roto-pulsating frame.

reach a target halo. Specifically, intersection in the configuration space is sought between the halo stable manifolds and a selenocentric transition orbit. Since the intersection occurs only in configuration space, a maneuver is necessary for orbital continuity. This maneuver places the spacecraft on the stable manifold of the target halo and is thus called stable manifold injection maneuve, Δv_{SMIM}. The transfer phase starts when the SMIM is executed, and ends after the halo injection maneuver, Δv_{HIM}, inserts the S/C into the target halo orbit. The aim of the transfer design analysis is to find the parameters of the selenocentric transition orbit and the stable manifold that lead to a minimum Δv_{SMIM} at the intersection. The optimization problem is stated as a nonlinear programming problem (NLP) method and then solved with Matlab active-set algorithm. The transfer parameters to quasi-halo generated by $C_j = 3.09$ are shown in Tab. 5. As expected, the SMIM occurs at the periselene of the transition orbit, i.e., $\theta \cong 0 \deg$. The transition orbit inclination lies within the parking orbit bounds, and no plane change maneuver is necessary.

Tab. 5: Main parameters for the transfer phase.

Parameter	Value
h_p [km]	200
h_a [km]	14964.2
i [deg]	78.1
Ω [deg]	30.0
ω [deg]	301.2
θ [deg]	~0
T [hrs]	22.42551
t_{po} [-]	0.7406
t_{sm} [-]	7.5397

3.3 Station-keeping on quasi-halo orbit

Considering the limited Δv capability, propellant consumption for station-keeping (S/K) on the operative orbit is a critical factor for mission sustainability. Using the generated quasi-halo orbits as reference trajectories, an effort is directed toward the development of a station-keeping strategy that can be used to maintain CubeSats near such nominal libration point orbits (LPO). The S/K cost is estimated by employing the target points method (TPM) first introduced in [14], then adapted to the problem of LPO by [15], and finally used for JAXA's EQUULEUS mission analysis [16]. A massive Monte-Carlo simulation is performed with 10000 samples, considering the impact of the injection, tracking, and maneuver execution processes on the nominal orbit determined in the presence of solar radiation pressure and gravity of the main solar system celestial bodies (i.e., Sun, 8 planets, the Moon, and Pluto). The errors on orbit injection, orbit determination, and the maneuver execution are all modeled and generated with zero-mean Gaussian distributions, where position, velocity, and maneuver offset covariances are set to 10 km, 10 cm/s, and 2%, respectively. This is compliant with the expected navigation performances [17]. The TPM parameters and the S/K maneuver epochs are fine-tuned for the LUMIO specific application with a direct simulation technique.

Tab. 6 displays the 1-year S/K cost with 1σ, 2σ, and 3σ confidence. The Monte-Carlo data is fitted by means of an inverse Gaussian distribution. As expected, the S/K cost increases for smaller (i.e., higher Jacobi constant) quasi-halos. This trend reflects the stability (eigenspectrum of the monodromy matrix) properties of halo orbits. That is, a larger halo is generally less unstable and thus cheaper to maintain.

Tab. 6: Confidence for the 1-year station-keeping cost.

C_j [-]	S/K cost [m/s]		
	1σ	2σ	3σ
3.09	18.3	23.9	28.1

3.4 LUMIO operative orbit

Fig. 6 shows the total transfer cost for different halos. The cost includes S/K, SMIM, and plane change maneuvers. It is conjectured the reason why the transfer cost has a clear-cut minimum area is twofold: for high energy levels (low Jacobi constant), the stable manifold
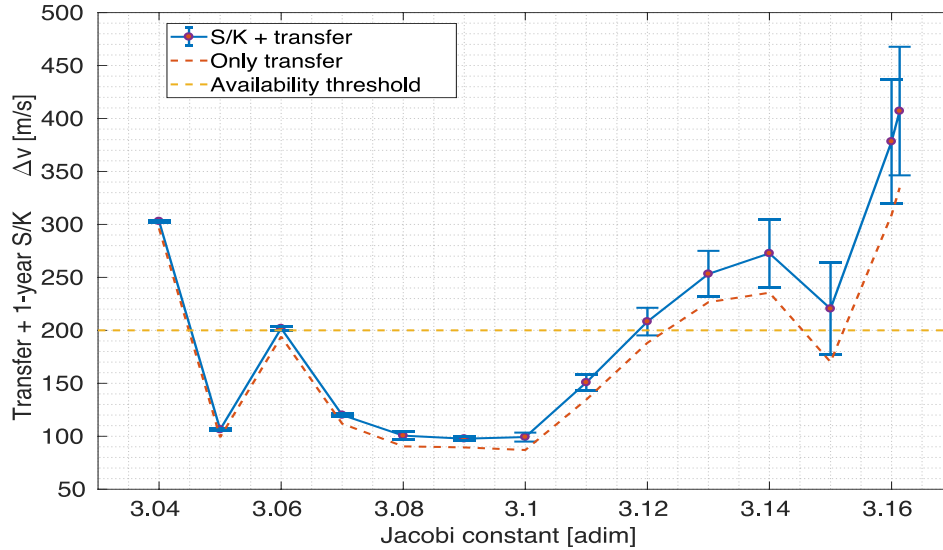
Fig. 6: Total transfer cost for different halos.

configuration space does not get close enough to the Moon to permit intersection with the selenocentric transition orbit; while for high Jacobi constant values, the stable manifolds cross the lunar region sufficiently close to provide patching opportunities with a selenocentric transition orbit, but the velocity mismatch is comparatively large, that is the outbound stable manifold is much faster than the S/C at periselene.

The quasi-halo generated for $C_j = 3.09$ is the designated LUMIO operative orbit. The selection of the LUMIO operative orbit is based on results of Fig. 6. Indeed, the quasi-halo is located at the center of a minimum plateau for total transfer cost which provides both a) optimality of maneuvers cost, and b) robustness against errors in the actual energy level of the injected stable manifold.

Mission Δv budgets for each maneuver and phase are reported in Tab. 7 with both deterministic and confidence values. The 1σ total cost is 154.4 m/s, which is also in line with a 12U CubeSat volume and mass budgets. Note that Item MAT-DV-14 of [18] states that stochastic maneuvers shall be calculated based on the 3σ confidence interval with no additional margins. The choice to consider a 1σ confidence interval on stochastic maneuvers for LUMIO is motivated by the inherently higher risk of a low-cost mission. Nonetheless, the overall stochastic Δv computed based on a 95.32% confidence level of a combination of all stochastic maneuvers is smaller than the linear sum by 19%. With this approach, the 3σ Δv budget sums up to 191.3 (195.5 with margins on SMIM, HIM, and disposal maneuver), which is still within the bounds for mission feasibility.

Tab. 7: Mission Δv budgets.

Maneuver	Cost [m/s]			
	Deterministic	1σ	2σ	3σ
PCM	0	-	-	-
Transition S/K	-	8	8	8
SMIM	89.47	-	-	-
TCM1	-	28.6	53.0	73.1
TCM2	-	6.5	15.0	24.8
HIM	0.5	-	-	-
1-year S/K	0	18.3	23.9	28.1
Disposal	3	-	-	-
TOTAL	**154.4**		**192.9**	**227.0**

4. System

The LUMIO spacecraft has been designed to perform with a high level of autonomy, particularly the navigation, payload data processor, and command data handling system (CDHS). The choice is driven not only by the operational constraints with respect to the lunar orbiter, but also by the ambitious mission design. Additionally, a general zero-redundancy approach has been adopted for all subsystems. This is dictated by the tight mass and volume constraints and a CubeSat design driven risk approach.

In subsystem design, a systematic trade-off procedure is adopted, based on subsystem specific performance criteria, as well as standard performance, cost and schedule criteria. Consistent design margins have been used for sizing the subsystems based on the development status. A standard 5%, 10%, and 20% mass margins have been applied for a fully COTS solution, a COTS solution requiring modification, and a custom design, respectively. The most important system and sub-system requirements are summarized in Tab. 8.

Tab. 8: Main system and subsystem requirements.

OVRSYS-1	The S/C mass shall be less than 24 kg
OVRSYS-2	The S/C volume shall be less than 12U and fit into a 12U CubeSat
OVRSYS-3	The system shall operate in standalone mode for10 days without communication
PROP-1	The propulsion system shall provide at least 154.39 m/s for S/K, orbital transfer, EoL disposal, and a minimum total impulse of 72.91 Ns for de-tumbling and wheel de-saturation
PROP-2	The maximum thrust of the propulsion system shall be 500 mN
PROP-3	The maximum thrusting time shall be of 8 hours per orbital transfer maneuver
ADCS-1	After the deployment, the ADCS shall de-tumble the spacecraft from tip-off rates of up to 30 deg/s in each axis
ADCS-3	The ADCS shall point with an accuracy of 0.1 deg during science and navigation phases
ADCS-5	The ADCS shall provide minimum pointing stabilization of 79.90 arcsec/s during the science phase
ADCS-6	The ADCS shall provide a maximum slew rate of 1 deg/s
EPS-1	The EPS shall supply 22 W average and 36 W peak power to the subsystems in the parking orbit phase
EPS-2	The EPS shall supply 23 W average and 39 W peak power to the subsystems during the transfer phase
EPS-3	The EPS shall supply 27 W average and 46 W peak power to the subsystems in science mode
EPS-4	The EPS shall supply 22 W average and 42 W peak power to the subsystems in navigation mode
EPS-5	The EPS shall have a mass less than 3 kg
COMMS-1	The spacecraft shall be able to receive telecommands from the lunar orbiter at the frequency range of 390-405 MHz
COMMS-2	The S/C shall send telemetry to the lunar orbiter at frequency range 435-450 MHz
COMMS-3	The S/C shall send payload data to lunar orbiter at frequency range 435-450 MHz
COMMS-4	The maximum available time limit for communication between the S/C and the lunar orbiter shall be 1 hour per day
PDLPROC-1	The payload processor shall receive and process a maximum 15 images per seconds from the optical payload
PDLPROC-2	The payload processor shall store a maximum of 13 MB of payload data per 29-days period to the COMMS for transmission to lunar orbiter

4.1 Propulsion

The trade-off related to the propulsion subsystem shows that chemical propulsion is the only feasible option for the main maneuvers (orbital transfer and station-keeping), since all other options pose serious risks in terms of mass, volume, and/or thrust level requirements. For the de-tumbling and de-saturation maneuvers, a clear preference should be given to a chemical or a cold gas system. The initial proposed design is based on a partially customized version of the VACCO Hybrid ADN MiPS, including one main mono-propellant thruster (ADN green propellant) providing a thrust of 0.1 N for the main maneuvers, plus four cold gas reaction control system (RCS) thrusters in a pyramid configuration, providing a thrust of 10 mN each for the de-tumbling and de-saturation maneuvers. Mission requirements can be accomplished with a propulsion system having a total wet mass of 5.6 kg and a total volume of 3.1U. Alternatives based on performing all required functions with the same propulsion type (mono-propellant or resistojet), as well as systems based on sole European developments, are to be investigated and better assessed during the next mission design phases.

4.2 Attitude determination and control

The preliminary architecture of the attitude determination and control (ADCS) subsystem for LUMIO is shown in Fig. 7. The sensor suite has been chosen by selecting those with the smallest mass, volume, and power budgets given the pointing requirements and tip-off rates in Tab. 8.
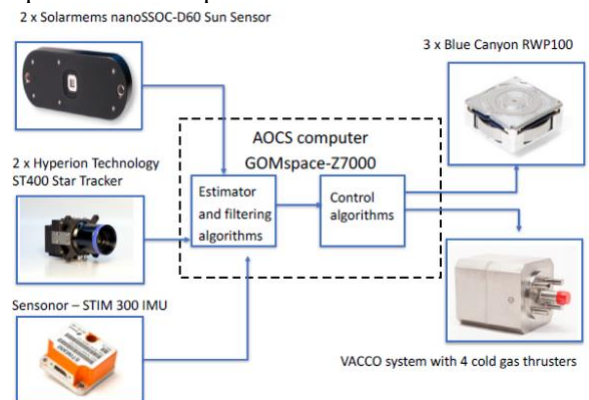

Fig. 7:ADCS architecture of the LUMIO spacecraft.

The sensor suite comprises a nano SSOC-D60 Sun sensor manufactured by Solar MEMs technology (43x14x5.9 mm, 6.5 g, accuracy of 0.5 deg 3σ, and precision of 0.1 deg), two ST400 star trackers manufactured by Hyperion Technologies and Berlin Space Technologies (53.8x53.8x90.5 mm, 280 g, accuracy of 10 arcsec 3σ in pitch and yaw, and 120 arcsec 3σ in roll axis), and a STIM300 ultra-high performance inertial measurement unit manufactured by Sensonor10 (33 cm³, 55 g). The on-board computer is the GOMspace-

Z7000, also used for the navigation algorithm. The actuators comprise 3 Blue Canyon RWP-100 reaction wheels (RW) and the set of cold gas RCS thrusters included in the VACCO propulsion system. The Blue Canyon RWP-100 reaction wheels are assumed to operate at a maximum of 90 mNms despite their capability of 100 mNms momentum storage. The ADCS system has a mass of 2 kg and a volume of 1150 cm^3.

4.3 Power

For the solar array assembly, GOMspace Nanopower MPS in its B-type configuration has been chosen, holding 16 AzurSpace 3G30C solar cell assemblies in its deployable configuration (currently under development). The size is 30x20 cm, with a thickness of 3.5 mm and a mass of 620 g inclusive of the solar cells. The deployable solar array is attached to a solar array drive assembly (SADA). The deployment of the solar array is achieved using a yoke which in turn is connected to the SADA inside the spacecraft. The total battery capacity is 160 Wh, achieved with two GOMspace Nanopower BPX 80 Wh batteries.

For power conditioning and distribution, the GOMspace Nanopower P60 unit is selected. The interfaces between the electrical power system (EPS) and the other subsystems are schematized in Fig. 9. The total mass of the EPS is estimated at 2.9 kg.
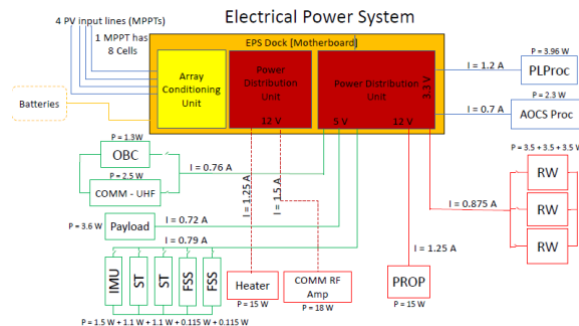

Fig. 9: Electrical interfaces between the EPS and the other subsystems.

4.4 Communication

The communication subsystem is based on two UHF turnstile antennas developed by ISIS-space (one for uplink and one for downlink, considering that the typical turnstile antennas bandwidth is less than 15 MHz in the UHF band) and a RF power amplifier allowing for an RF output power of 8 W, necessary given the high transmission power required to close the link at distances greater than 75000 km, expected during the mission. The UHF transponder is based on the Consultative Committee for Space Data Systems (CCSDS) Proximity-1 control, with RS442 data interface and a maximum data rate of 512 kbps. Tab. 9 shows the link budgets estimated for the current configuration of the communications subsystem. In the operation phase, the PL/TM throughput is 25919 kB for a 29-day period with 16 one-hour communication slots. This means that, when the minimum payload data requirement of 12927 kB is met, the data budget available for telemetry is 12992 kB.

Tab. 9:Telemetry, telecommand, and payload link budget.

Link	TM return link	Payload data return link	TC Feeder link	Unit
Frequency	435	435	390	MHz
Modulation and coding	BPSK, Rate 1/2, K=7	BPSK, Rate 1/2, K=7	BPSK, Rate 1/2, K=7	-
Transmitter RF Power	8	8	2	W
Antenna (Gr/T)	-17.4	-7.8	-17.4†	-
Range	75000	75000	74400	km
Data Rate	1000	8000	1000	bps
Free Space Loss	182.7	182.7	181.7	dB
Received Eb/No	7.52	8.09	8.01	dB
Required Eb/No (BER=10^{-6})	5	5	5	dB
Margin	2.52	3.09	3.01	dB

† Conservative estimate since receiver details are not known. (Receiver at 60000 km from transmitter).

4.5 Structure

The main satellite structure is a COTS-based 12U CubeSat structure produced by ISIS-space. A detailed radiation analysis is conducted to define the thickness of the satellite external aluminum panels for sufficient radiation shielding, taking as a reference the LUMIO operative orbit and the position of the Moon for 1 year. The SPENVIS solar particle model ESP-PSYCHIC (total fluence) is used to calculate the total ionizing dose (TID) and long-term Single Event Upsets for the operational orbit. Then, using the SHIELDOSE-2 model, the TID is plotted as a function of the thickness of aluminum shielding material of the spacecraft (refer to
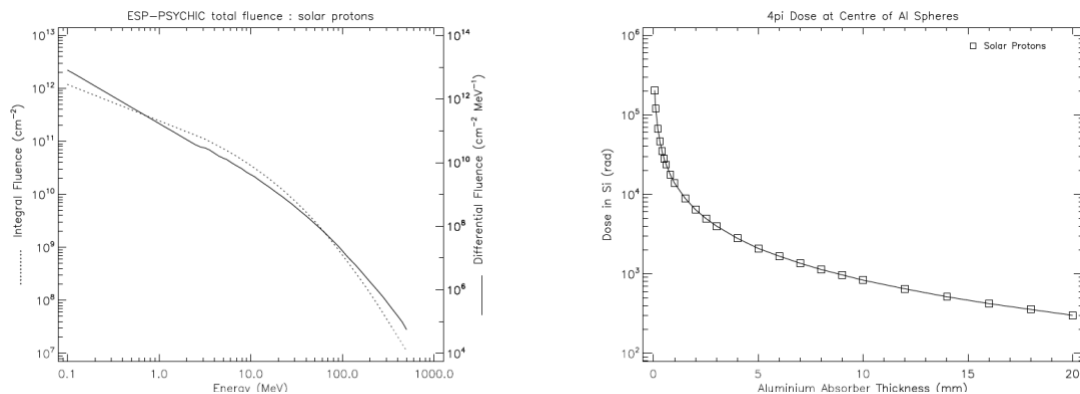

Fig. 8: Radiation analysis for 1-year geocentric circular orbit of 435000 km radius, starting on August 22, 2023.

Fig. 8). Since most of the internal spacecraft components can tolerate a TID up to 20 krad, and applying a 100% margin on this value due to large uncertainties at this stage, a thickness of 1.5 mm is selected, with additional internal shielding foreseen for particularly critical components (IMU, star trackers, SADA). The total mass of the structure designed with this criterion is 4 kg. The QuadPack deployer from ISIS-space is expected to be used for deploying the CubeSat from the lunar orbiter.

4.6 Thermal analysis

A simplified steady-state single-node thermal analysis is conducted with the main spacecraft body and the solar arrays considered as different thermally isolated bodies. Given the large uncertainties in the spacecraft internal and external design, the analysis is performed in a low-fidelity model and environment. Results show that, with a combination of thermal coatings of 27% gold, 25% silvered Teflon, and 48% polished Al 6061-T6, the spacecraft temperature stays within the range -5 to +45 deg Celsius when illuminated by the Sun. During eclipse periods, temperatures of roughly -50 deg are estimated, which may require the use of internal heaters for further thermal protection of the most critical components.

4.7 Command and data handling and on-board payload data processor

The selected on-board computer (OBC) for the LUMIO spacecraft is the AAC Microtec Sirius computer, equipped with RS-422 and RS-485 connections as well as two SpaceWire 10 Mbps links, a 32-bit fault tolerant CPU and an EDAC protected memory. A CAN bus is foreseen for the connection with the ADCS and payload dedicated computers, as well as the EPS; although the selected computer does not support it natively, an option is available for accommodate a CAN-compatible transceiver upon request. The connection with the communication subsystem is done with RS-422, the only type of link supported by the UHF transponder. For the dedicated OBPDP, the GOMspace Nanomind Z7000 processor is selected. The OBPDP is connected to the camera through a SpaceWire interface, and to the main spacecraft OBC and dedicated ADCS computer through a CAN bus. This configuration allows for handling the required frame rate of 15 fps with a size of approximately 2 MB per frame.

4.8 Spacecraft configuration

Fig. 10 shows the current foreseen configuration for the LUMIO spacecraft, while the complete mass budget, including margins at system and subsystem level, is shown in Tab. 10. A total margined mass of ~21.1 kg is estimated for the spacecraft. Additional mass may be used for deviating from the zero-redundancy strategy by adding components to avoid single points of failure, for including additional propellant to extend the mission

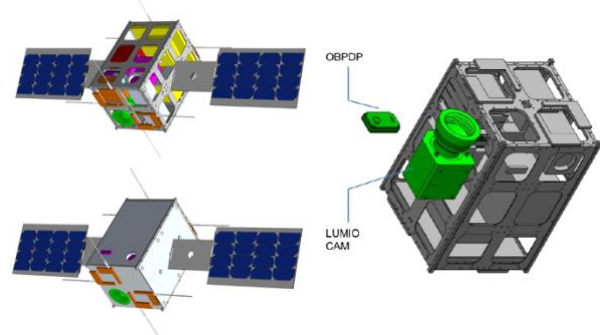lifetime, or for accommodating additional payloads to exploit secondary mission objectives.

Fig. 10: LUMIO without and with panels (left), and exploded view showing LUMIO-Cam (right).

Tab. 10: Mass budget of the LUMIO spacecraft, including system and subsystem margin.

Component	Mass [kg]	Design approach	Margin [%]
Payload	1.3	Custom design	20
Payload processor	0.2	Full COTS	5
Propulsion	5.6	Modified COTS	10
Communication	0.5	Custom design	20
CDHS	0.3	Modified COTS	10
ADCS	2.0	Full COTS	5
EPS	2.9	Modified COTS	10
Structure	4.0	Modified COTS	10
Thermal	0.1	Modified COTS	10
Electrical harness	0.5	Modified COTS	10
Overall margin			**10**
TOTAL MASS	**21.1**		

5. Conclusions

The primary science goal of LUMIO mission is to observe meteoroid impacts on the lunar farside to study the characteristics of meteoroids and to improve the meteoroid models. This may lead to a further study of the sources of these meteoroids, such as asteroids in the near-Earth environment and comets. The LUMIO mission complements ground-based observations with remote space-based observations, so improving the lunar situational awareness. The mission utilizes a 12U form-factor CubeSat which carries the LUMIO-Cam, an optical instrument capable of detecting light flashes in the

visible and NIR spectrum to continuously monitor and process the data. The mission implements a novel orbit design and the latest CubeSat technologies to serve as a pioneer in demonstrating how CubeSats can become a viable tool for deep space science and exploration.

In this paper, an assessment on LUMIO payload, mission analysis, and subsystems is performed. An independent assessment conducted at ESA's Concurrent Design Facility also indicates mission feasibility, and has identified possible delta-design options, which will be considered in the next phases of the mission design.

Acknowledgements

References

[1] Z. Ceplecha *et al.*, "Meteor Phenomena and Bodies," *Sp. Sci. Rev.*, vol. 84, no. 3, pp. 327–471, 1998.

[2] P. Brown, R. E. Spalding, D. O. ReVelle, E. Tagliaferri, and S. P. Worden, "The flux of small near-Earth objects colliding with the Earth.," *Nature*, vol. 420, no. 6913, pp. 294–296, 2002.

[3] J. L. Ortiz *et al.*, "Detection of sporadic impact flashes on the Moon: Implications for the luminous efficiency of hypervelocity impacts and derived terrestrial impact rates," *Icarus*, vol. 184, no. 2, pp. 319–326, 2006.

[4] T. V Gudkova, P. H. Lognonné, and J. Gagnepain-Beyneix, "Large impacts detected by the Apollo seismometers: Impactor mass and source cutoff frequency estimations," *Icarus*, vol. 211, no. 2, pp. 1049–1065, 2011.

[5] R. M. Suggs, D. E. Moser, W. J. Cooke, and R. J. Suggs, "The flux of kilogram-sized meteoroids from lunar impact monitoring," *Icarus*, vol. 238, no. Supplement C, pp. 23–36, 2014.

[6] J. Oberst *et al.*, "The present-day flux of large meteoroids on the lunar surface--A synthesis of models and observational techniques," *Planet. Space Sci.*, vol. 74, no. 1, pp. 179–193, 2012.

[7] F. Cipriano, A. M. and Dei Tos, D. A. and Topputo, "Orbit Design for LUMIO: The Lunar Meteoroid Impacts Observer," *Front. Astron. Sp. Sci.*, vol. 5, no. 29, pp. 1--23, 2018.

[8] S. Bouley *et al.*, "Power and duration of impact flashes on the Moon: Implication for the cause of radiation," *Icarus*, vol. 218, no. 1, pp. 115–124, 2012.

[9] L. R. Bellot Rubio, J. L. Ortiz, and P. V Sada, "Luminous Efficiency in Hypervelocity Impacts from the 1999 Lunar Leonids," *Astrophys. J. Lett.*, vol. 542, no. 1, pp. L65--L68, 2000.

[10] R. M. Suggs, W. J. Cooke, R. J. Suggs, W. R. Swift, and N. Hollon, "The NASA Lunar Impact Monitoring Program," *Earth. Moon. Planets*, vol. 102, no. 1, pp. 293–298, 2008.

[11] A. Z. Bonanos *et al.*, "NELIOTA: ESA's new NEO lunar impact monitoring project with the 1.2m telescope at the National Observatory of Athens," in *Proceedings of the International Astronomical Union*, 2015, vol. 10, no. S318, pp. 327–329.

[12] D. A. Dei Tos and F. Topputo, "On the advantages of exploiting the hierarchical structure of astrodynamical models," *Acta Astronaut.*, vol. 136, pp. 236–247, 2017.

[13] D. A. Dei Tos and F. Topputo, "Trajectory refinement of three-body orbits in the real solar system model," *Adv. Sp. Res.*, vol. 59, no. 8, pp. 2117--2132, 2017.

[14] N. P. Dwivedi, "Deterministic optimal maneuver strategy for multi-target missions," *J. Optim. Theory Appl.*, vol. 17, no. 1, pp. 133–153, 1975.

[15] K. C. Howell and H. J. Pernicka, "Stationkeeping method for libration point trajectories," *J. Guid. Control Dyn.*, vol. 16, p. 151, 1993.

[16] K. Oguri *et al.*, "EQUULEUS mission analysys: design of the science orbit phase," in *26th International Symposium on Space Flight Dynamics*, 2017, no. 72, pp. 1–7.

[17] V. Franzese, P. Di Lizia, and F. Topputo, "Autonomous Optical Navigation for LUMIO Mission," in *2018 Space Flight Mechanics Meeting, AIAA SciTech Forum*, 2018, pp. 1–11.

[18] SRE-PA & D-TEC staff, "Margin philosophy for science assessment studies," 2012.

[19] C. H. Acton Jr, "Ancillary data services of NASA's navigation and ancillary information facility," *Planet. Space Sci.*, vol. 44, no. 1, pp. 65–70, 1996.

[20] C. H. Acton Jr, N. Bachman, B. Semenov, and E. Wright, "A look towards the future in the handling of space science mission geometry," *Planet. Space Sci.*, vol. 150, pp. 9–12, 2018.